Biomaterials 305 (2024) 122448

Contents lists available at ScienceDirect

Biomaterials

journal homepage: www.elsevier.com/locate/biomaterials

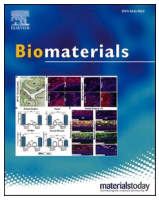

Use of oxygen-loaded nanobubbles to improve tissue oxygenation: Bone-relevant mechanisms of action and effects on osteoclast differentiation☆

Helen J. Knowles [a], Alexandra Vasilyeva [a,b], Mihir Sheth [a,b], Oliver Pattinson [c], Jonathan May [c], Robin M.H. Rumney [d], Philippa A. Hulley [a], Duncan B. Richards [a], Dario Carugo [a], Nicholas D. Evans [c], Eleanor Stride [a,b,*]

[a] Botnar Institute for Musculoskeletal Sciences, Nuffield Department of Orthopaedics Rheumatology & Musculoskeletal Sciences, University of Oxford, Oxford, UK
[b] Institute of Biomedical Engineering, Department of Engineering Science, University of Oxford, Oxford, UK
[c] Bone and Joint Research Group, Human Development and Health, Faculty of Medicine, University of Southampton, Southampton General Hospital, Southampton, UK
[d] School of Pharmacy and Biomedical Sciences, University of Portsmouth, UK

ARTICLE INFO

Keywords:
Nanobubble
Oxygen
Monocyte
Osteoclast
Osteoclastogenesis
Fusion

ABSTRACT

Gas-loaded nanobubbles have potential as a method of oxygen delivery to increase tumour oxygenation and therapeutically alleviate tumour hypoxia. However, the mechanism(s) whereby oxygen-loaded nanobubbles increase tumour oxygenation are unknown; with their calculated oxygen-carrying capacity being insufficient to explain this effect. Intra-tumoural hypoxia is a prime therapeutic target, at least partly due to hypoxia-dependent stimulation of the formation and function of bone-resorbing osteoclasts which establish metastatic cells in bone. This study aims to investigate potential mechanism(s) of oxygen delivery and in particular the possible use of oxygen-loaded nanobubbles in preventing bone metastasis via effects on osteoclasts. Lecithin-based nanobubbles preferentially interacted with phagocytic cells (monocytes, osteoclasts) via a combination of lipid transfer, clathrin-dependent endocytosis and phagocytosis. This interaction caused general suppression of osteoclast differentiation via inhibition of cell fusion. Additionally, repeat exposure to oxygen-loaded nanobubbles inhibited osteoclast formation to a greater extent than nitrogen-loaded nanobubbles. This gas-dependent effect was driven by differential effects on the fusion of mononuclear precursor cells to form pre-osteoclasts, partly due to elevated potentiation of RANKL-induced ROS by nitrogen-loaded nanobubbles. Our findings suggest that oxygen-loaded nanobubbles could represent a promising therapeutic strategy for cancer therapy; reducing osteoclast formation and therefore bone metastasis via preferential interaction with monocytes/macrophages within the tumour and bone microenvironment, in addition to known effects of directly improving tumour oxygenation.

1. Introduction

Hypoxia, defined as a reduction in tissue oxygenation resulting in oxygen demand exceeding oxygen supply, is a common feature of solid tumours that drives tumour progression and is predictive of poor clinical outcome. Hypoxia is considered a prime therapeutic target; either via strategies to directly increase the oxygen content of tumour tissue [1] or via targeting the hypoxia-inducible factor (HIF) transcription factor that regulates the hypoxic transcriptional cascade [2].

Hypoxia within the primary tumour promotes metastasis to distant sites via mechanisms including the promotion of angiogenesis, migration and invasion, and the formation of cancer stem cells and tumour

☆ Eleanor Stride reports financial support was provided by Engineering and Physical Sciences Research Council. Helen Knowles reports financial support was provided by National Institute for Health and Care Research. Mihir Sheth reports financial support was provided by Gilberto Sayao da Silva. Helen Knowles reports financial support was provided by UK Spine. Eleanor Stride has patent #512728.5 licensed to Avrox Technologies Ltd. If there are other authors, they declare that they have no known competing financial interests or personal relationships that could have appeared to influence the work reported in this paper.

* Corresponding author. Botnar Research Centre, Nuffield Orthopaedic Centre, University of Oxford, Oxford, OX3 7LD, UK.
E-mail address: eleanor.stride@eng.ox.ac.uk (E. Stride).

https://doi.org/10.1016/j.biomaterials.2023.122448
Received 31 July 2023; Received in revised form 14 December 2023; Accepted 21 December 2023
Available online 28 December 2023

cell-derived extracellular vesicles [3,4]. Primary tumours commonly metastasise to the skeleton. Many breast, prostate and lung cancer patients develop bone metastases, which cause significant morbidity owing to hypercalcaemia, fracture and bone pain; major contributors to a poor quality of life and to poor prognosis [5]. Additional hypoxia-dependent mechanisms establish metastatic cells in bone; especially the initiation of the "vicious cycle" whereby cancer cells disrupt physiological bone homeostasis by stimulating osteoclast formation and enhancing bone resorption, thus releasing bone-derived factors which in turn stimulate growth of the metastatic tumour [6].

Osteoclasts are multi-nucleated cells that resorb bone, which form by the fusion of $CD14^+$ monocytic precursors in the presence of macrophage colony stimulating factor (M-CSF) and receptor activator of nuclear factor kappa B ligand (RANKL) [7,8]. *In vitro*, intermittent hypoxia (cyclic hypoxia and reoxygenation) stimulates osteoclast formation from murine and human precursor cells, with maximal effect at 2% O_2 [9–12]. Indeed, acute hypoxia increases bone resorption by mature osteoclasts via inhibition of the HIF-regulating prolyl hydroxylase domain 2 (PHD2) enzyme and induction of HIF-1α [9,13–15]. In contrast, chronic exposure to either low oxygen [12] or chemically-induced hypoxia [16] inhibits osteoclastogenesis and causes extensive osteoclast death.

These oxygen-dependent effects on osteoclasts may also play a role in establishing bone metastasis in cancer. Transcutaneous treatment of tibially implanted MDA-MB-231 human breast cancer cells with 100% CO_2 increases intratumour oxygenation, reducing expression of HIF-1α as well as reducing the number and activity of tumour-resident osteoclasts and inhibiting metastatic bone destruction [17]. Additionally, high expression of hypoxia-induced lysyl oxidase (LOX) in human primary colorectal tumours is associated with poor clinical outcome. Overexpression of LOX in murine colorectal tumours promotes the formation of osteolytic lesions via RANKL-dependent induction of osteoclastogenesis and tumour cell dissemination to the bone [18]. Reducing tissue hypoxia in the primary tumour, as well as at the metastatic site, might therefore be expected to have beneficial effects on outcome measures via inhibitory effects on osteoclasts.

Gas-filled microbubbles stabilised by a biocompatible lipid shell have been used medically for decades as ultrasound contrast agents [19]. More recently, they are being exploited for therapeutic drug delivery and as a method of oxygen delivery to increase tumour oxygen levels [20–22]. Smaller diameter oxygen 'nano'bubbles, a term widely used to denote bubbles <500 nm in diameter, show similar effects [23,24]. Using an orally-delivered suspension of surfactant-stabilised oxygen nanobubbles, we have recently shown a reduction in tumour hypoxia in a BxPC-3 xenograft tumour model of human pancreatic cancer. Oxygen nanobubbles cause a 25% reduction in intratumoural HIF-1α protein as well as reduced expression of HIF-regulated vascular endothelial growth factor (VEGF) mRNA [25]. The increase in tumour oxygenation caused by exposure to oxygen nanobubbles prior to sonodynamic therapy is sufficient to enhance the efficiency of the therapy and further reduce tumour growth [26]. Oxygen nanobubbles also reduce tumour size and inhibit expression of HIF-1α in mice bearing 4T1 breast cancer tumours [27], with MB49 bladder cancer tumours additionally showing reduced levels of hypoxyprobe and reversion of the methylation status in hypoxic tumour regions [28]. Encouragingly, oral administration of the same nanobubbles to human athletes also shows a beneficial effect on performance during intense exercise when tissue oxygenation is a limiting factor [29].

Intriguingly, however, calculations suggest that the oxygen-carrying capacity of the nanobubbles should not be sufficient to explain this level of effect. The quantity of encapsulated oxygen delivered in a 0.2 ml nanobubble dose is estimated as only approximately 0.002 mg oxygen, insufficient to explain the persistent measured changes in tumour oxygenation *in vivo* [26]. The current study aims to investigate potential mechanism(s) of oxygen delivery by assessing interaction of nanobubbles with different skeletally-relevant cell types *in vitro*. Liposomes have been widely investigated for phagocyte-targeted therapies as they are naturally cleared by the mononuclear phagocyte system, especially smaller liposomes of <100 nm [30]. Lipid-based oxygen nanobubbles might therefore also interact preferentially with monocytes/macrophages within the tumour and bone microenvironment. Consequently, this study will also investigate the feasibility of using oxygen-loaded nanobubbles to reduce osteoclast formation, an outcome which could potentially prevent bone metastasis alongside improvements in tumour oxygenation.

2. Materials and methods

2.1. Materials and ethics

Unless stated, reagents were from Merck Life Science (Gillingham, UK). Oxygen and nitrogen gas cylinders were purchased from BOC (Guilford, Surrey, UK). Elephant dentine was obtained from HM Revenue & Customs (Heathrow Airport, UK). Use of leucocyte cones (NHS Blood and Transplant) was approved by the London–Fulham Research Ethics Committee (11/H0711/7). Human osteoblasts were obtained from surgical waste tissue (HTA Licence No. 12217, Oxford REC C 09/H0606/11). The study was conducted in accordance with the Declaration of Helsinki.

2.2. Nanobubble preparation

Nanobubbles were prepared in a modification of the method of Owen et al. [25]. Briefly, glycyrrhizic acid (0.5 mg/ml), soybean lecithin (3 mg/ml), citric acid (5 mg/ml) and glycerol (1.25% (v/v)) were mixed in Dulbecco's PBS and stirred for 45 min on a hot plate at 90–100 °C. The solution was then agitated by shaking for 1 min. 10 ml of nanobubble suspension was transferred to a 50 ml vial and sparged with oxygen or nitrogen gas for 3 min after which the headspace was filled with the same gas and the vial tightly sealed. Air nanobubbles were unsparged. Gas-sparged PBS was prepared by following the same procedure with PBS instead of a nanobubble sample. Nanobubbles were freshly prepared for each experiment and were used immediately after gas-sparging at a final concentration ranging from 1 to 10%, indicating the volume of NB suspension added as a percentage of the media volume.

The size distributions and concentrations of the nanobubble suspensions were measured using Interference Light Microscopy (ILM) (VideoDrop, Myriade, FR) (Suppl Fig. S1). Zeta Potential was measured using the Laser Doppler Velocimetry on the ZetaSizer Nano ZS (Malvern Panalytical, USA). The nanobubble suspension was diluted in PBS 1:100, and pH balanced to 7.4. Due to the high conductivity of 16.6–17.9 mS/cm, monomodal analysis was used to calculate the mean Zeta Potential across 10–100 measurement runs per reading. For each sample, 3 readings were taken at 25 °C.

2.2. Culture of primary human monocytes and osteoclasts

$CD14^+$ monocytes were positively selected from the PBMC fraction of leucocyte cones using magnetic $CD14^+$ microbeads (Miltenyi Biotech, Bisley, UK). Monocytes were seeded at 0.25×10^6 cells/well into 96-well plates (containing 4 mm diameter dentine discs for resorption assays) or at 1×10^6 cells/well into 24-well plates in α-MEM (without ribonucleosides/deoxyribonucleosides) containing 10% FBS (v/v), 2 mM L-glutamine, 50 IU/ml penicillin and 50 μg/ml streptomycin sulphate. For monocyte culture, cells were maintained in 25 ng/ml M-CSF (R&D Systems, Abingdon, UK). Alternatively, osteoclastogenesis was induced after overnight incubation in αMEM by addition of 25 ng/ml M-CSF and 50 ng/ml RANKL (Peprotech, London, UK). Media and cytokines were replenished every 3–4 days for up to 10 days.

2.3. Cell culture

The MG-63 human osteoblastic osteosarcoma cell line was obtained from the EuroBoNeT cell line biobank [31]. The BxPC3 human pancreatic adenocarcinoma cell line was purchased from the ATCC (Manassas, VA, USA). MG-63 and BxPC-3 cells were maintained in RPMI-1640 media supplemented with 10% FBS, L-glutamine (2 mM), penicillin (50 IU/ml) and streptomycin sulphate (50 μg/ml) in a humidified atmosphere at 37 °C (5% CO_2 in air). Human Umbilical Vein Endothelial Cells (HUVEC) were obtained from Invitrogen and cultured in M199 media with Endothelial Cell Growth Supplement (R&D Systems) and were used up to passage 6.

Primary human osteoblasts were obtained from bone fragments (approx. 1 mm^2) that were washed in PBS then incubated in 1 mg/ml collagenase at 37 °C for 30 min before incubation in a 10 cm dish in α-MEM containing 10% (v/v) FBS, 2 mM Glutamax, 50 IU/ml penicillin and 50 μg/ml streptomycin sulphate. After 2 days, media was replaced and additionally supplemented with 5 μg/ml ascorbate-2-phosphate. Supplemented media was replaced every 3–4 days and outgrowth osteoblasts were banked in liquid nitrogen once confluence was reached. Osteoblasts were used up to passage 5.

Primary human $CD19^+$ B cells and $CD3^+$ T cells were selected from the PBMC fraction of leucocyte cones using magnetic $CD19^+$ or $CD3^+$ microbeads (Miltenyi Biotec). Cells were maintained overnight in α-MEM and used for experiments the following day.

Hypoxic exposures were performed in 0.5% or 2% O_2, 5% CO_2, balance N_2 in a MiniGalaxy incubator (RS Biotech, Irvine, UK).

2.4. Observing cell-nanobubble interaction

Nanobubbles were labelled with the fluorescent lipid-analogue dye DiO (0.35 μg/μl; Invitrogen) at 37 °C for 20 min. DiO-labelled nanobubbles were added to cells in media and incubated for up to 24 h. For mechanistic experiments, cells were pre-incubated for 20 min with 80 μM dynasore, 250 μM monodansylcadaverine, 30 μM nystatin, 2.5 mM methyl-β-cyclodextrin, 5 μM 7-keto cholesterol (Cayman Chemical), 15 μM cytochalasin D, 20 μM chloroquine, 5 μM lantrunculin B (Cayman Chemical) or vehicle control prior to application of nanobubbles. For confocal microscopy, cells were labelled with Cell Mask Deep Red (CMDR; Invitrogen) by incubation with 1 μl CMDR/ml media for 30 min at 37 °C and then washed in PBS prior to incubation with nanobubbles.

2.4.1. Flow cytometry

Cells were washed with PBS and incubated in Accutase at 37 °C for 5–45 min (dependent on cell type). Cells were then centrifuged at 350 g for 5 min, resuspended in FACS buffer (PBS, 0.5% (w/v) BSA, 2 mM EDTA) at 1×10^7 cells/ml, and analysed immediately on a BD Fortessa calibrated with calibration and tracking beads. 10,000 events were recorded per sample using FACS Diva software (BD Biosciences). Data were analysed using FlowJo 10.8.1 software (BD Biosciences, Wokingham, UK).

2.4.2. Confocal microscopy

Images for the interaction between DiO-labelled nanobubbles and Cell Mask Deep Red-labelled cells were acquired on Zeiss LSM 710 and LSM 980 confocal microscopes (Carl Zeiss AG, Oberkochen, Germany) using a 63× objective and ZEN Black software (Zeiss).

2.5. Osteoclast quantification assays

2.5.1. TRAP staining

Formalin-fixed osteoclasts were stained for tartrate-resistant acid phosphatase (TRAP) using naphthol AS-BI phosphate as a substrate with reaction of the product with fast violet B. Equal volumes of solution A (10 mg naphthol AS-BI phosphate, 0.5 ml DMSO in 15 ml acetate-tartrate solution [0.2 M acetic acid, 0.2 M sodium acetate, 10 mM sodium tartrate, pH5]) and solution B (20 mg fast violet B salt, 0.5 ml DMSO in 15 ml acetate tartrate solution) were mixed and incubated on fixed cells for 3 h at 37 °C in the dark prior to washing and air drying. Photographs were obtained on a Nikon Eclipse TE300 microscope with an Axiocam 105 camera (Carl Zeiss AG) and ZEN acquisition software (blue edition; Zeiss). Multinucleated cells with three or more nuclei were considered osteoclasts.

2.5.2. Vitronectin receptor (VNR) staining

Immunostaining for osteoclast-specific VNR used an anti-CD51/61 antibody (clone 23C6, 1:400; BioRad, Oxford, UK) and standard DAB immunohistochemistry techniques.

2.5.3. Bone resorption

Osteoclasts were removed from dentine discs by sonication and resorption tracks were visualised by staining with 0.5% (w/v) toluidine blue in boric acid. Dentines were photographed on an Olympus BX40 microscope with ZEN (blue edition) acquisition software. For quantification, resorption tracks were highlighted in Adobe Photoshop and the relative resorbed area was measured using ImageJ software (Fiji; National Institutes of Health, Bethesda, USA).

2.4.2. Cell viability and metabolic activity

Alamar blue (BioRad) fluorescence was measured as an indicator of cell viability. Alternatively, following overnight seeding, cells were incubated in media supplemented with 0.5 μM SYTOX™ Green Nucleic Acid Stain (ThermoFisher Scientific, Loughborough, UK). The green fluorescent (Ex/Em 504/523 nm) signal from dead cells was detected using an Incucyte S3 (Sartorius, Goettingen, Germany) and normalised to cell number obtained from phase contrast images using the associated software. The concentration of glucose and glutamine in conditioned media was measured using the Glucose (GO) Assay Kit and Glutamine/Glutamate Determination Kit (Merck Life Science) according to the manufacturer's instructions.

2.4.3. Western blotting

Cells were sonicated in lysis buffer (6.2 M urea, 10% glycerol, 5 mM dithiothreitol, 1% sodium dodecyl sulphate, protease inhibitors) before the cell extract was separated by 8% SDS-PAGE and transferred onto a PVDF membrane. Membranes were incubated overnight with primary antibodies specific HIF-1α (clone 54, 1:1000; BD Biosciences, Oxford, UK), GLUT1 (ab14683, 1:2500; Abcam, Cambridge, UK) or β-tubulin (clone TUB2.1, 1:2500, Sigma-Aldrich, Dorset, UK). Chemiluminescence was detected using a UVITEC Alliance Q9 gel doc system and densitometry was performed in ImageJ, normalizing experimental bands to the corresponding β-tubulin control.

The VEGF concentration in conditioned media was quantified using the human DuoSet ELISA kit against VEGF (DY293B; R&D Systems) according to the manufacturer's instructions.

2.4.4. Measurement of intracellular ROS

Cells were incubated with CM-H2DCFDA (Invitrogen) for 20 min at 37 °C, washed in PBS and then incubated in αMEM additionally supplemented with nanobubbles and/or ROS inducers (100 ng/ml RANKL, 200 ng/ml PMA). Green fluorescence indicative of intracellular ROS was measured after 10 min and 1 h incubation using an Incucyte S3.

2.4.5. Microbubble preparation

Lipid films were prepared by evaporation of $CHCl_3$ from a 9:1 mixture of DBPC (1,2-behenoyl-*sn*-glycero-3-phosphatidylcholine): DSPE-PEG2000 (1,2-distearoyl-*sn*-glycero-3-phosphoethanolamine-*N*-[methoxy (polyethylene glycol)-2000] (ammonium salt) (Avanti Polar Lipids/Merck). Lipids were resuspended in PBS at 4 mg/ml by stirring for 45 min on a hot plate at 85–90 °C, then sonicated for 2 min at 40% amplitude using a probe sonicator positioned at the bottom of the liquid. Using a bespoke lid allowing access of the sonicator probe, the

headspace was filled with O_2 or N_2 gas applied at a low flow rate for 5 min after which a second sonication at the liquid/gas interface for 30 s (70% amplitude power) was used to generate the microbubbles. The vessel was then sealed, transferred to an ice bath for 10 min and used immediately. Microbubble size and concentration were quantified by optical microscopy. A 10 μL MB sample was pipetted into a haemocytometer (Hausser Scientific Company) under a 24 mm × 24 mm glass coverslip (VWR International). MBs were imaged at 40× magnification using a Leica DM500 microscope (Leica Microsystems GmbH, Germany) coupled with a CCD camera (Leica Microsystems GmbH, Germany). Microbubble sizing and counting were performed using purpose-written code in MATLAB® analysing approximately 40 images (The Mathworks, Natick, USA).

3. Statistics

For graphical data, the number of experimental repeats is represented by the number of data points; error bars indicate one standard deviation of the mean. Data was analysed using GraphPad Prism (GraphPad Software, La Jolla, CA, USA). Normality tests were D'Agostino Pearson or Shapiro–Wilk, depending on the sample size. Statistical analysis comprised one-way or two-way ANOVA using Dunnett's or Tukey's multiple comparison or Kruskal–Wallis ANOVA with Dunn's multiple comparison. For experiments with only two conditions, a T test or Mann–Whitney test was applied. Results were considered significant at $p < 0.05$.

4. Results

4.1. Nanobubbles preferentially interact with phagocytic cells

To begin to assess the mechanism of gas delivery by nanobubbles, as well as to identify cells that could mediate musculoskeletal effects relevant to bone metastasis, air nanobubbles (NB-air) were incubated with a panel of skeletally-relevant cell types including primary human $CD14^+$ monocytes, osteoclasts, $CD3^+$ T cells, $CD19^+$ B cells and osteoblasts (HOb), endothelial cells (HUVEC) and the MG-63 osteoblastic cell line. BxPC-3 prostate cancer cells were also included, to assess whether recent effects of NB on hypoxia in the primary tumour *in vivo* might be due to NB interaction with cancer cells, stromal cells or both [25]. Cells were exposed to 5% (v/v) NB-air labelled with the fluorescent lipophilic stain DiO for up to 24 h before cell-nanobubble interaction was analysed by flow cytometry. Only phagocytic cells (monocytes, osteoclasts, HUVECs, T cells) showed substantial interaction with nanobubbles,

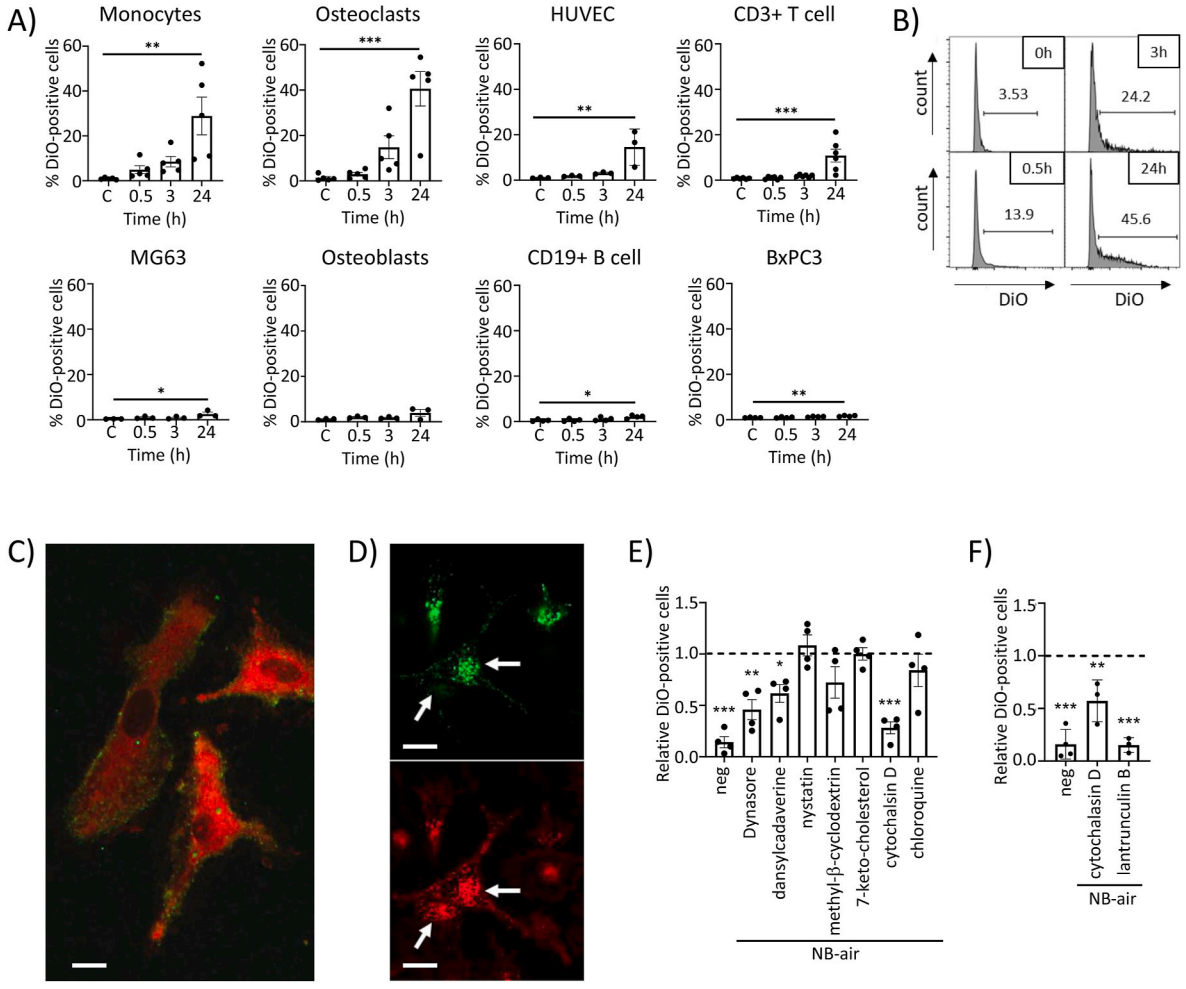

Fig. 1. Monocyte-nanobubble interactions involve lipid transfer, clathrin-dependent endocytosis and phagocytosis. (A, B) Flow cytometry of cells exposed to DiO-labelled NB-air for up to 24 h showing (A) the proportion of DiO-positive cells and (B) increased intensity of staining over time. (C, D) Confocal images of monocyte (red; cell mask deep red) interaction with NB-air (green; exposed to DiO) after (C) 3 h exposure (scale bar = 10 μm) and (D) 24 h exposure (scale bar = 20 μm). Arrows indicate a DiO-positive monocyte immediately adjacent to a DiO-negative cell. (E, F) Flow cytometry of monocytes treated with a panel of endocytosis and phagocytosis inhibitors for (E) 24 h or (F) 5 h alongside exposure to DiO-labelled NB-air. Dashed line indicates value of DiO-labelled NB-air positive control. Error bars indicate one standard deviation of the mean. Significance is either indicated by bars or relates to the positive control; *$p < 0.05$, **$p < 0.01$, ***$p < 0.001$. (For interpretation of the references to color in this figure legend, the reader is referred to the Web version of this article.)

determined as a combination of statistical significance and the proportion of DiO-positive cells after 24 h being greater than 10% (Fig. 1a). Lack of nanobubble interaction with non-phagocytic cells was not due to loss of cell viability in these cells (Suppl Fig. S2). Incubation of monocytes with a DiO control diluted and incubated with PBS instead of NB-air confirmed that unbound DiO did not interact with the cells (Suppl Fig. S2).

Monocytes and osteoclasts exhibited the greatest interaction with nanobubbles despite high inter-donor variability (Fig. 1a). A large proportion of cells did not interact with the NB-air and there was considerable variation in intensity of staining, especially at later timepoints (Fig. 1a and b). Confocal microscopy revealed that the initial interaction of monocytes with nanobubbles involved lipid transfer of the DiO-labelled NB-air with the cell membrane, giving rise to a punctate appearance in the cell membrane after 3 h exposure (Fig. 1c). After 24 h, DiO-positive monocytes in which intracellular nanobubbles were present to a highly variable extent could be observed immediately adjacent to DiO-negative cells (Fig. 1d).

To investigate whether active uptake is involved in interactions of cells with nanobubbles, monocytes were treated with a panel of endocytosis and phagocytosis inhibitors prior to 24 h incubation with DiO-labelled NB-air. Interaction of nanobubbles with monocytes was inhibited by dynasore, dansylcadaverine, cytochalasin D and lantrunculin B, indicative of an involvement of clathrin-dependent endocytosis and phagocytosis (Suppl Fig. S3; Fig. 1e and f).

4.1.1. *Nanobubbles have moderate gas-dependent effects on monocyte viability*

As differential effects of the gas-loading of nanobubbles on tissue oxygenation are evident *in vivo*, we investigated whether gas-dependent effects could be observed *in vitro* in monocytes or osteoclasts, the two cell types exhibiting greatest interaction with nanobubbles. Nanobubbles were either unsparged (NB-air) or loaded with nitrogen (NB–N_2) or oxygen (NB–O_2) gas.

In $CD14^+$ monocytes, low dose NB-N_2 (1–2.5% v/v) caused a 32–43% reduction in cell number after 72 h when compared with either NB-O_2 or NB-air (Fig. 2a) in the absence of any effect on cell death (Fig. 2b), suggesting that NB-N_2 reduce the rate of monocyte proliferation. This gas-dependent effect was lost at higher doses (5–10% v/v) due to a strong general nanobubble-dependent suppression of cell number and increased cell death (Fig. 2a and b). Hypoxic conditions (0.5% O_2) also caused a strong reduction in cell number (Fig. 2c; dashed line; 0.17 $\pm$ 0.04, $p < 0.001$, relative to normoxic control) with little effect on cell viability (Fig. 2d), again indicative of a reduced rate of proliferation. Only small gas-dependent effects of nanobubbles were evident under hypoxia, with some indication that NB-N_2 further increased cell death in comparison with NB-O_2, although with no significant reduction in cell number (Fig. 2c and d).

In osteoclasts, stronger and highly variable nanobubble-dependent effects on cell death (Suppl Fig. S4) initiated a reduction in duration of exposure from 72 h to 24 h. High dose nanobubbles reduced the number of osteoclasts and increased cell death in both normoxic and hypoxic conditions, but no gas-dependent effects of nanobubbles were observed under any conditions when cultured on either cell culture plastic (Fig. 2e–h) or dentine discs (Suppl Fig. S5).

4.1.2. *Nanobubbles show strong gas-dependent effects on osteoclast differentiation*

Intermittent hypoxia (cyclic hypoxia and reoxygenation) promotes osteoclast differentiation from monocytic precursors [9–12] and we hypothesised that gas-loaded nanobubbles might mimic this effect; with NB-N_2 mimicking transient hypoxia by reducing cellular oxygen tension to promote osteoclastogenesis and NB-O_2 having the opposite effect. Exposure to nanobubbles on days 1, 3 and 6 of osteoclastogenesis caused strong nanobubble-dependent suppression of osteoclast formation at all doses after 9 days (Fig. 3a), due to inhibition of cell-cell fusion by the nanobubbles (Fig. 3b) and/or loss of viability of any osteoclasts that do form. Additionally, at low nanobubble doses (1% v/v) a gas-dependent

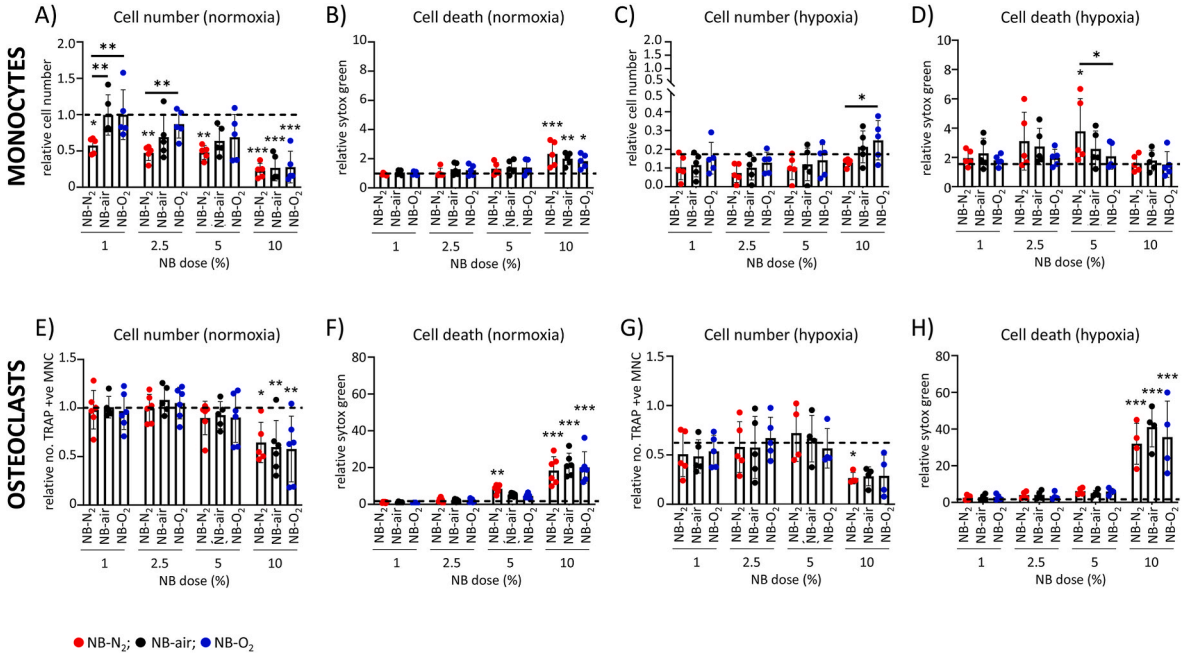

Fig. 2. Effects of gas-loaded nanobubbles on cell number and viability of monocytes and osteoclasts. (A–D) Monocytes cultured for 72 h with 1–10% (v/v) nanobubbles and assessed for (A, C) cell number or (B, D) cell death under either (A, B) normoxic or (C, D) hypoxic (0.5% O_2) conditions. (E–H) Osteoclasts cultured for 24 h with 1–10% (v/v) nanobubbles and assessed for (E, G) cell number or (F, H) cell death under either (E, F) normoxic or (G, H) hypoxic (2% O_2) conditions. Red = NB-N_2, black = NB-air, blue = NB-O_2. Dashed lines indicate either the normoxic (no-nanobubble) control value of 1.0 or, under hypoxic conditions, the value of the hypoxic (no-nanobubble) control in relation to the normoxic control value of 1.0. Error bars indicate one standard deviation of the mean. Significance is either indicated by bars or relates to the no-nanobubble control; *$p < 0.05$, **$p < 0.01$, ***$p < 0.001$. (For interpretation of the references to color in this figure legend, the reader is referred to the Web version of this article.)

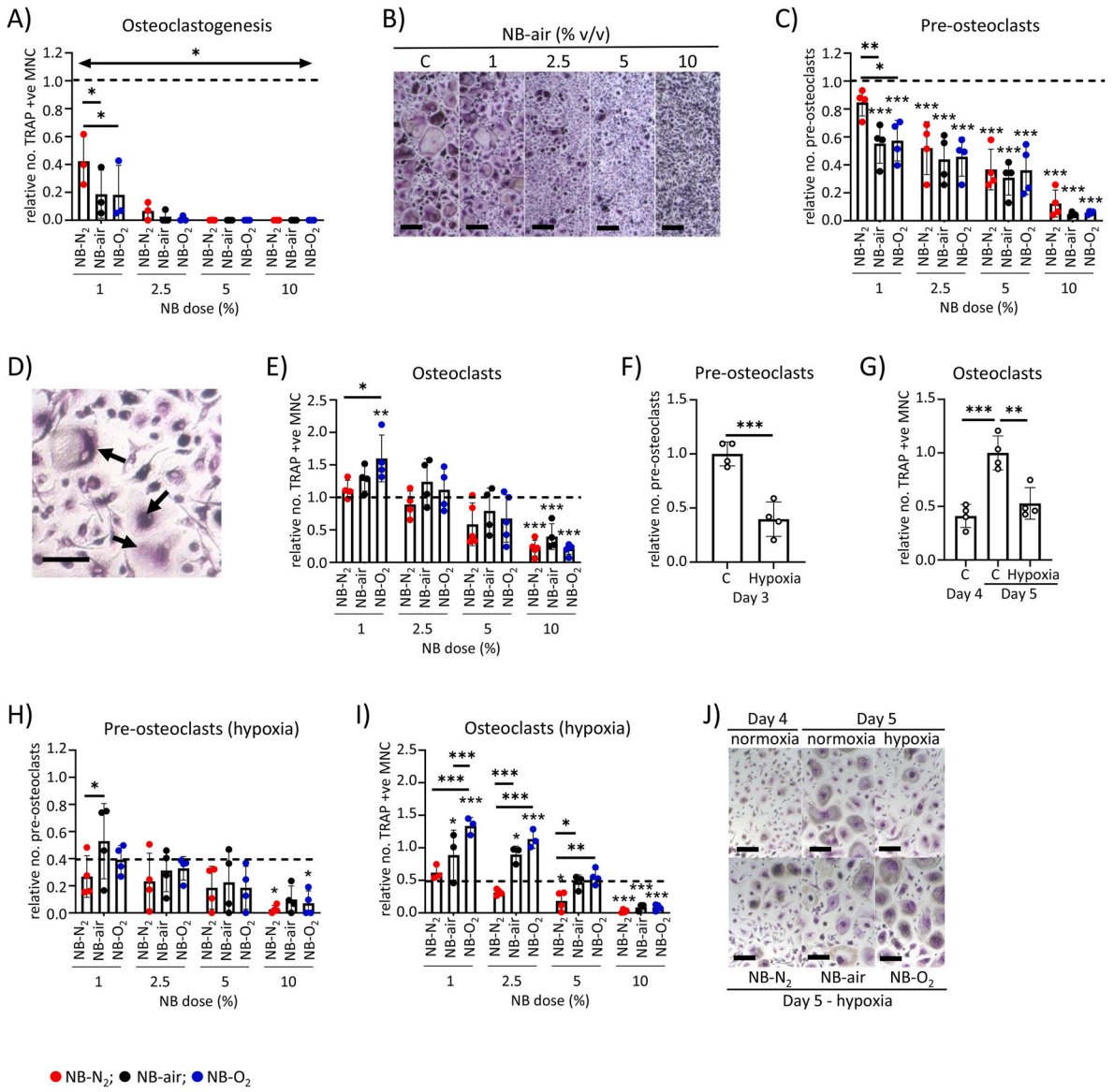

Fig. 3. NB-O_2 inhibit osteoclast differentiation. (A, B) TRAP staining of osteoclasts formed on day 9 of differentiation, with addition of 1–10% (v/v) nanobubbles on day 1, 3 and 6; (A) quantification of the number of TRAP-positive cells with 3 or more nuclei, (B) representative images demonstrating reduced fusion (scale bars = 100 μm). (C, D) TRAP staining of pre-osteoclasts formed on day 3 or 4 (donor dependent) of differentiation, with addition of 1–10% (v/v) nanobubbles on day 1; (C) quantification of the number of TRAP-positive cells with 2 nuclei; (D) representative image with arrows indicating binuclear pre-osteoclasts (scale bar = 50 μm). (E) Quantification of the number of TRAP-positive cells with 3 or more nuclei formed on day 5 or 6 (donor dependent) of differentiation, with addition of 1–10% (v/v) nanobubbles on day 4 or 5. (F, G) Effect of hypoxia on the formation of (F) pre-osteoclasts (day 1–3 or 1–4, 2% O_2) and (G) osteoclasts (day 4–5 or 5–6, 2% O_2). (H–J) Effect of 1–10% (v/v) nanobubbles on the formation of (H) pre-osteoclasts and (I) osteoclasts under hypoxic (2% O_2) conditions. (J) Representative images showing effects of nanobubbles on osteoclast formation under hypoxia (scale bars = 100 μm). Red = NB-N_2, black = NB-air, blue = NB-O_2. Dashed lines indicate either the normoxic (no-nanobubble) control value of 1.0 or, under hypoxic conditions, the value of the hypoxic (no-nanobubble) control in relation to the normoxic control value of 1.0. Error bars indicate one standard deviation of the mean. Significance is either indicated by bars or relates to the no-nanobubble control; *$p < 0.05$, **$p < 0.01$, ***$p < 0.001$. (For interpretation of the references to color in this figure legend, the reader is referred to the Web version of this article.)

effect was evident where NB-O_2 and NB-air caused greater inhibition of osteoclast formation than NB-N_2 (Fig. 3a).

Osteoclastogenesis involves sequential fusion processes; initial fusion of two mononuclear cells to generate binuclear pre-osteoclasts, followed by fusion between the resulting multinucleated cells and other mononuclear cells to produce larger osteoclasts with 3 or more nuclei [32]. We next investigated the effect on nanobubbles of these distinct fusion processes. Under normoxic culture conditions, single exposure to nanobubbles during the initial fusion stage (from day 1–3 or day 1–4) caused dose-dependent inhibition of pre-osteoclast formation (Fig. 3c and d). Again, the 1% (v/v) dose of NB-O_2 or NB-air caused greater inhibition of the formation of pre-osteoclasts than NB-N_2 (Fig. 3c). Interestingly, the opposite gas-dependent effect occurred during later fusion to form multi-nucleated osteoclasts. Following a single 24 h exposure to nanobubbles (day 4–5 or 5–6), a 1% (v/v) dose of NB-O_2 caused the formation of more osteoclasts than NB-N_2 (Fig. 3e). Therefore, the additional inhibitory effect of NB-O_2 on overall osteoclast differentiation appears to be driven primarily by inhibition of the fusion of mononuclear cells to form pre-osteoclasts.

Exposure to hypoxia (2% O_2) inhibited both the initial fusion to form pre-osteoclasts (Fig. 3f) and subsequent fusion events (Fig. 3g). Nanobubbles did not affect pre-osteoclast formation under hypoxia; no substantial nanobubble-dependent or gas-dependent effects were observed (Fig. 3h). However, hypoxic inhibition of the formation of mature

osteoclasts was completely abrogated by NB-O_2 at all but the highest nanobubble doses, while NB-N_2 had a further inhibitory effect (Fig. 3i and j). Application of PBS-N_2 and PBS-O_2, gas-loaded in the same manner as the nanobubbles, confirmed that the observed gas differential was due to gas-loading of the nanobubbles rather than dissolved gas in the buffer (Suppl Fig. S4).

4.2. Gas-dependent effects of nanobubbles are not driven by HIF

HIF-1α is the main transcription factor driving the cellular response to hypoxia [33]. Primary human monocytes and osteoclasts were incubated with gas-loaded nanobubbles for 16 h under either normoxic or hypoxic conditions and analysed for expression of HIF-1α and HIF-regulated proteins. In monocytes, a general nanobubble-dependent increase in HIF-1α and HIF-regulated Glut-1 was evident in hypoxic conditions (Fig. 4a), although this did not reach significance for HIF-1α (Fig. 4b). Secretion of HIF-regulated VEGF increased in a nanobubble-dependent manner in both normoxia and hypoxia (Fig. 4c), suggesting that even the non-significant increase in HIF-1α is sufficient to activate HIF-mediated transcription in these cells.

In contrast, nanobubble exposure of osteoclasts had no discernible effect on HIF-1α, Glut-1 or VEGF protein under either normoxic or hypoxic conditions (Fig. 4d–f). Additionally, gas-loaded nanobubbles did not affect the rate of consumption of glucose or glutamine in either normoxic or hypoxic conditions in either cell type (Suppl Fig. S6).

Effects on the HIF transcriptional pathway, therefore, do not obviously explain the gas-dependent effect of nanobubbles on osteoclast differentiation.

4.3. A potential role for reactive oxygen species (ROS)

The osteoclast differentiation factor RANKL generates intracellular ROS in osteoclast precursor cells, causing an increase in RANKL-mediated signalling which drives osteoclastogenesis and bone resorption [34,35]. ROS are also upregulated due to the presence of hypoxia in tumour tissue [36]. We confirmed that intracellular ROS levels increased during monocyte-osteoclast differentiation (Fig. 5a) and that addition of exogenous RANKL caused an immediate transient increase in ROS in monocytes (Fig. 5b). Incubation of monocytes with nanobubbles for 1 h caused a nanobubble-dependent increase in intracellular ROS at high doses (5–10% v/v) (Fig. 5c), but no significant increase was seen at the low (1% v/v) nanobubble dose where gas-dependent effects on osteoclast formation occurred. Interestingly, RANKL stimulation immediately after addition of 1% v/v nanobubbles caused a >10-fold increase in ROS levels after 1 h, with an indication of a greater effect with NB-N_2 than NB-air or NB-O_2 (Fig. 5d). This effect was amplified by use instead of PMA, a more potent ROS-inducer than RANKL (Fig. 5e), which caused a gas-dependent 144-fold increase in ROS production with NB-N_2, almost 2-fold greater than that produced by either NB-air or NB-O_2 (Fig. 5f). Given the role of ROS in osteoclast formation, elevated potentiation of RANKL-induced ROS by NB-N_2 could explain the greater osteoclast formation seen with these nanobubbles in comparison with NB-O_2 (Fig. 3a, c).

Lecithin-mediated lipid transfer is necessary for inhibitory effects of nanobubbles on cell fusion events during osteoclastogenesis

We next investigated which nanobubble component(s) drives general nanobubble-mediated suppression of osteoclast fusion events. The citric acid in the nanobubble formulation results in acidification of cell culture media, even at low doses (Fig. 6a). Inhibitory effects on the number (Fig. 6b) and viability (Fig. 6c) of monocytic precursor cells were lost when citric acid was removed from the formulation. Removal of citric acid also prevented cell death in the more sensitive osteoclast population (Fig. 6d). However, in the absence of citric acid nanobubble-dependent inhibition of cell fusion still resulted in negligible osteoclast formation at high nanobubble doses despite reduced cytotoxicity (Fig. 6e). Crucially, citric acid-depleted nanobubbles retained gas-dependent effects on overall osteoclast differentiation (Fig. 6e) and on secondary fusion events under hypoxia (Fig. 6f).

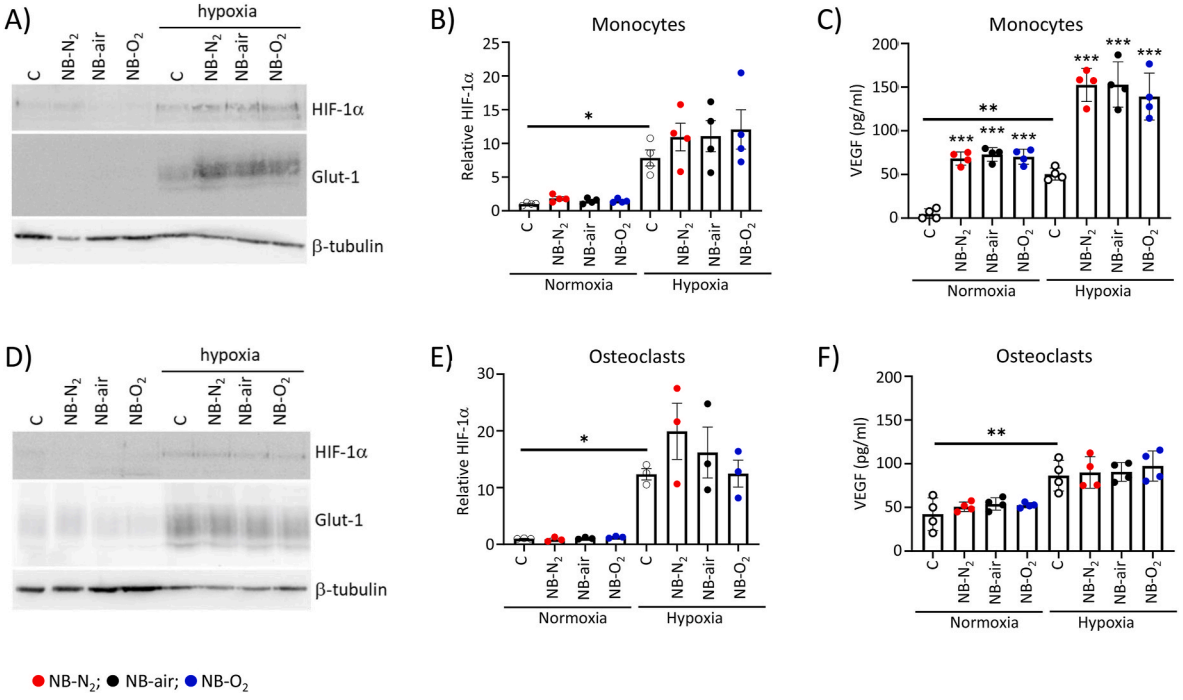

Fig. 4. No gas-dependent effect of nanobubbles on HIF. Monocytes (A–C) and osteoclasts (D–F) incubated with 1–10% (v/v) nanobubbles for 16 h under either normoxic or hypoxic conditions were assessed for (A, D) expression of HIF-1α and Glut-1 protein by Western blot, with (B, E) HIF-1α levels quantified by densitometry, and (C, F) secretion of VEGF by ELISA. Red = NB-N_2, black = NB-air, blue = NB-O_2. Error bars indicate one standard deviation of the mean. Significance is either indicated by bars or relates to the relevant normoxic or hypoxic control; *p < 0.05, **p < 0.01, ***p < 0.001. (For interpretation of the references to color in this figure legend, the reader is referred to the Web version of this article.)

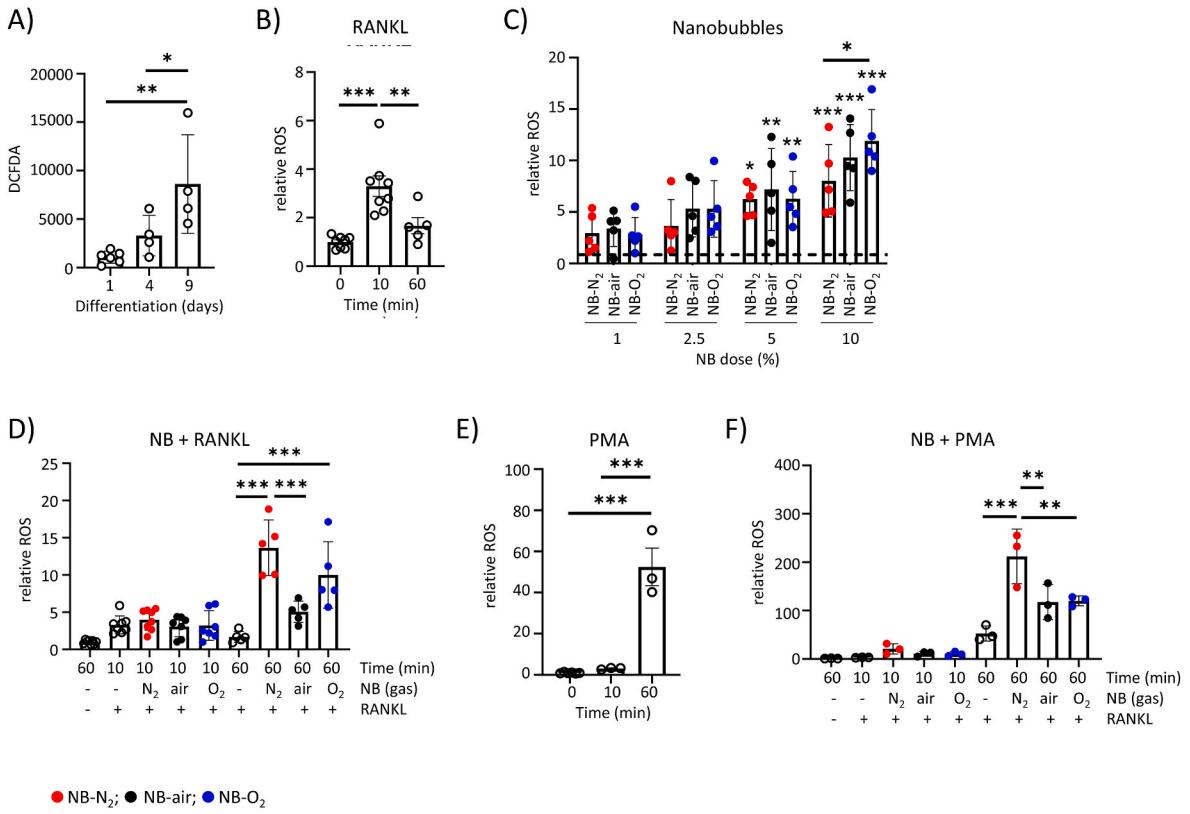

Fig. 5. NB-N_2 induce most ROS in combination with other ROS-inducing agents. Measurement of intracellular ROS in monocytes: (A) on day 1, 4 and 9 of differentiation into osteoclasts; (B) after stimulation with 100 ng/ml RANKL; (C) after incubation with 1–10% (v/v) gas-loaded nanobubbles for 1 h; (D) after incubation with 1% (v/v) gas-loaded nanobubbles and 100 ng/ml RANKL for 10 min or 60 min; (E) after stimulation with 200 ng/ml PMA; and (F) after incubation with 1% (v/v) gas-loaded nanobubbles and 200 ng/ml PMA for 10 min or 60 min. Red = NB-N_2, black = NB-air, blue = NB-O_2. Dashed lines indicate the normoxic (no-nanobubble) control value of 1.0. Error bars indicate one standard deviation of the mean. Significance is either indicated by bars or relates to the relevant normoxic or hypoxic control; *p < 0.05, **p < 0.01, ***p < 0.001. (For interpretation of the references to color in this figure legend, the reader is referred to the Web version of this article.)

We therefore considered whether lecithin-dependent lipid transfer from nanobubbles to osteoclast precursor cells could be disrupting the fusion events necessary for osteoclast formation. Removal of lecithin from the nanobubble mix prevented the formation of 'particles' in the suspension (Suppl Fig. S7) and removed any inhibition of osteoclast formation, even at the highest doses (Fig. 6g), implying the requirement for lipid bubbles to be present in order to inhibit osteoclast formation.

To further test the hypothesis that cell-nanobubble interaction has a general inhibitory effect on osteoclast formation, we compared monocyte-osteoclast differentiation in cells exposed to the gas-loaded nanobubbles (NB–N_2, NB-O_2) with those exposed to gas-loaded microbubbles of a contrasting size and formulation (MB-N_2, MB-O_2) (Table 1). The higher dose (2.5% v/v) of both micro and nanobubbles caused general bubble-dependent suppression of osteoclast formation. Both nanobubbles and microbubbles also exhibited a gas-dependent effect, whereby the low (1% v/v) dose of oxygen-loaded bubbles caused greater inhibition of osteoclast formation than nitrogen-loaded bubbles (Fig. 6h).

5. Discussion

The results above show that lecithin-based nanobubbles preferentially interacted with professional phagocytes > non-professional phagocytes > non-phagocytic cells. Exposure of monocytes to nanobubbles caused general suppression of cell-cell fusion during osteoclast differentiation that was accentuated by exposure to NB-O_2 in comparison with NB-N_2. These observations have multiple mechanistic and therapeutic implications.

Physical interaction of nanobubbles with monocytes involved punctate lipid transfer to the cell membrane, as well as later intracellular uptake via clathrin-dependent endocytosis and phagocytosis. It is well known that cells of the mononuclear phagocyte system that includes monocytes and macrophages preferentially phagocytose liposomes, especially those containing negatively charged lipids such as phosphatidylserine [30]. For reference, in this study the zeta potential of the air nanobubbles was -28.12 ± 1.76 mV. Clathrin-mediated endocytosis is also a common mechanism of uptake for nano-sized particles [37,38].

We have previously shown that phosphatidylcholine-based microbubbles loaded with the lipophilic dye DiI exhibit punctate lipid transfer to the cell membrane, a pattern potentially indicative of transfer via lipid vesicles or aggregates [39]. The punctate nature of the interaction is similar to that observed here with nanobubbles, although the nanobubble puncti are considerably smaller. The interaction was also similar in that lipid transfer from microbubbles did not occur with all cells in the population, as also occurs during interaction with nanodroplets [40]. Lipid transfer from the microbubbles changed the membrane properties of the interacting cells including increasing membrane viscosity and causing microbubble composition-dependent changes in lipid order [39].

It is interesting to speculate about how these nanobubble interactions might inhibit the cell-cell fusion necessary for osteoclast differentiation. Classically activated M1 macrophages are highly phagocytic. Interestingly, alternatively activated (M2) murine macrophages, but not M1 macrophages, can differentiate into functional osteoclasts [41,42]. Although M1 activation is not the same as active endo/phagocytosis, this might suggest that monocytes actively taking

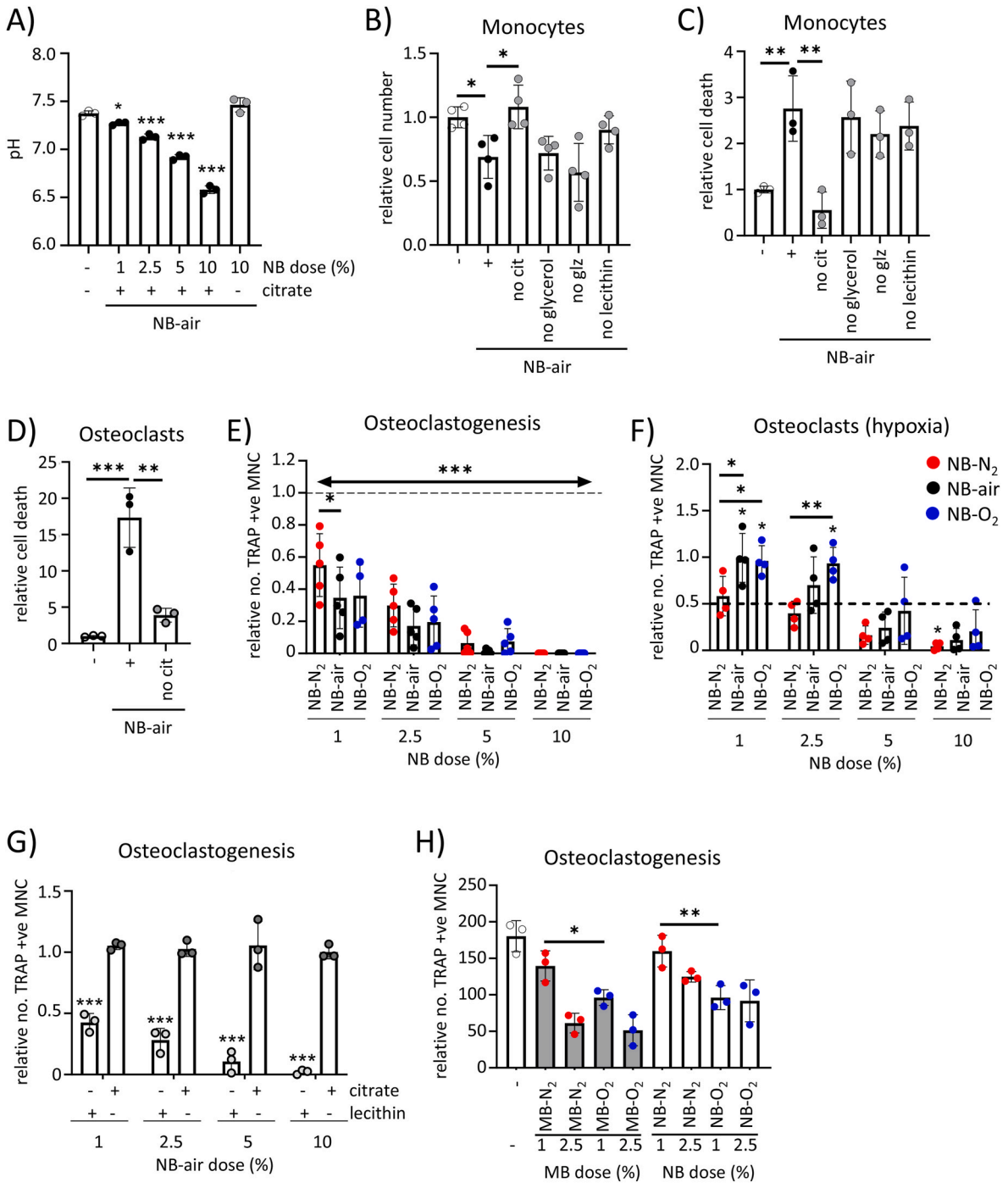

Fig. 6. Lipid transfer to cells drives inhibition of cell-cell fusion events. (A) pH measurements in cell culture media 10 min after addition of 1–10% (v/v) NB-air or NB-air lacking citric acid (no cit). (B–C) Monocytes cultured for 72 h with 10% (v/v) NB-air or NB-air lacking individual components (Cit = citric acid, glz = glycyrrhizic acid) and assessed for (B) cell number or (C) cell death. (D) Osteoclasts cultured for 24 h with 10% (v/v) NB-air or NB-air lacking citric acid and assessed for cell death. (E–F) Quantification of the number of TRAP-positive cells with 3 or more nuclei on (E) day 9 of differentiation, following addition of 1–10% (v/v) nanobubbles lacking citric acid on day 1, 3 and 6; (F) day 5 or 6 (donor dependent) of differentiation, following addition of 1–10% (v/v) nanobubbles lacking citric acid and exposure to hypoxia (2% O_2) on day 4 or 5. (G–H) Quantification of the number of TRAP-positive cells with 3 or more nuclei on day 9 of differentiation: (G) following addition of 1–10% (v/v) NB-air lacking either citric acid (white circles) or lecithin (black circles) on day 1, 3 and 6; (H) following addition of 1% or 2.5% (v/v) gas-loaded nanobubbles (white bars; NB-N_2, NB-O_2) or gas-loaded microbubbles (grey bars; MB-N_2, MB-O_2) on day 1, 3 and 6. Red = NB-N_2, black = NB-air, blue = NB-O_2. Dashed lines indicate either the normoxic (no-nanobubble) control value of 1.0 or, under hypoxic conditions, the value of the hypoxic (no-nanobubble) control in relation to the normoxic control value of 1.0. Error bars indicate one standard deviation of the mean. Significance is either indicated by bars or relates to the no-nanobubble control; *p < 0.05, **p < 0.01, ***p < 0.001. (For interpretation of the references to color in this figure legend, the reader is referred to the Web version of this article.)

Table 1
Differing size and formulation of nanobubbles and microbubbles.

	Nanobubbles (NB)	Microbubbles (MB)
Formulation	lecithin glycyrrhizic acid citric acid glycerol	1,2-behenoyl-*sn*-glycero-3-phosphatidylcholine (DBPC) 1,2-distearoyl-*sn*-glycero-3-phosphoethanolamine-*N*-[methoxy (polyethylene glycol)-2000] (DSPE-PEG2000)
Mean diameter	262.8 ± 78.1 nm	1.56 ± 0.76 μm

up nanobubbles are less likely to undergo osteoclast differentiation. However, other studies have shown that effects of particle phagocytosis by human macrophages on osteoclast differentiation are dependent on the composition of the ingested particles [43].

During osteoclastogenesis, fusion-committed osteoclast precursors display non-apoptotic phosphatidylserine at their surface. This phosphatidylserine exposure is necessary for cell-cell fusion via binding to extracellular annexin A5 and the formation of an annexin-based protein scaffold which regulates the fusogenic activity of syncitin-1 [44]. Multinucleation of preosteoclasts from murine bone marrow-derived macrophages is markedly inhibited by antibodies against either phosphatidylserine or its receptors (TIM4, BAI1, STAB2) [45]. Lecithin, the central phospholipid component of the nanobubbles in this study, is a mixture of glycerophospholipids including phosphatidylserine, phosphatidylcholine, phosphatidylethanolamine, phosphatidylinositol and phosphatidic acid. It is possible that free nanobubbles bind extracellular annexin A5 or phosphatidylserine receptors, competing for binding to pro-fusogenic phosphatidylserine on preosteoclasts. Alternatively, nanobubble-derived phosphatidylserine transferred into the cell membrane might interact with these proteins, again competing for binding to the pro-fusogenic form. The same mechanism(s) may also be true for the microbubbles in this study; phosphatidylcholine is also able to bind annexin A5 [46]. Additionally, alterations in the lipid concentration and/or composition of the cell membrane can affect its ability to co-localise signalling partners and so dramatically alter protein-lipid interactions at the membrane, including those that are involved in the translocation of receptors and signalling proteins to or from the cell membrane [47]. This could potentially include receptors involved in the highly regulated sequential fusion processes of osteoclastogenesis.

On top of general nanobubble-dependent suppression of osteoclast formation, fewer osteoclasts formed after repeat exposure to NB-O_2 than to NB-N_2. *In vitro*, osteoclast formation is enhanced by intermittent hypoxia (cyclic hypoxia and reoxygenation) [9–12]. It is possible that dosing every 3 days with NB-N_2 mimics intermittent hypoxia in this respect, resulting in the higher numbers of osteoclasts formed with NB-N_2 than with the other gas-loaded nanobubbles. This gas-dependent effect on overall osteoclast differentiation appeared to be driven by early effects on mononuclear cell fusion to form pre-osteoclasts, where acute exposure to NB-N_2 again caused the formation of more pre-osteoclasts than NB-O_2.

Intriguingly, acute exposure to nanobubbles during the later stages of osteoclast differentiation to form larger multi-nucleated cells exhibited the opposite gas-dependent effect; NB-O_2 caused the formation of more osteoclasts than NB-N_2, especially under hypoxic conditions. The sequential fusion that is characteristic of osteoclastogenesis comprises an initial fusion event between two mononuclear cells to form pre-osteoclasts, followed by fusion between the resulting multinucleated cells and other mononuclear cells. Different molecular mechanisms operate in each instance; CD47 promotes the fusion of mononuclear monocytes to form binuclear preosteoclasts, whereas syncytin-1 stimulates the generation of larger osteoclasts via fusion between mononuclear and multinucleated cells [32]. It is possible that the two fusion mechanisms respond differently to N_2 ('hypoxia') and O_2 ('reoxygenation'), with hypoxia promoting the formation of pre-osteoclasts and oxygenated conditions being required for the later stages of cell fusion. A gas-sensitivity such as this would explain the beneficial effect of hypoxia/reoxygenation on osteoclast differentiation over either condition alone [12].

Another possible mechanism for the gas-dependent effects observed during these later stages of osteoclast differentiation could be related to osteoclast fission. It has recently been shown that RANKL-stimulated mitophagy-dependent fission of osteoclasts generates smaller daughter cells called osteomorphs. Osteomorphs are more motile than large osteoclasts, enabling energy-conserving osteoclast recycling via later fusion of osteomorphs at different sites [48,49]. It is possible that hypoxia promotes osteoclast fission during the later stages of differentiation and that treatment with NB-O_2 prevents this fission. Investigations of osteoclast fission currently focus on mature osteoclasts rather than multi-nucleated but immature cells in the process of differentiation. However, effects of hypoxia on fission are unknown and it will be of interest to dissect the mechanisms further in future studies.

Most hypoxic transcriptional responses are directed by the transcription factor HIF. Given the very small amount of either O_2 or N_2 gas that can be carried in nanobubbles [26], and their interaction with only a minor proportion of cells in a population, it is unsurprising that effects on HIF were absent at a population level. However, it is possible that transient modulation of HIF might occur specifically in cells with which the nanobubbles directly interact and which are individually and acutely micro-dosed with gas. In the case of osteoclast differentiation, this might specifically cause gas-dependent changes in the fusion capacity of those directly interacting cells. It is possible that an improved HIF-1α response could be achieved *in vitro* via modification of the lipid composition of the nanobubbles. Khan et al. achieved effective reduction of HIF-1α in hypoxic MDA-MB-231 cells with an optimal combination of DSPC, DSPE-PEG-2000-Amine and DSPE-PEG-2000-Biotin at a molar ratio of 85:8:7 [50,51]; however, it is also possible that the ability to modulate HIF *in vitro* is cell type specific.

An alternative gas-dependent mechanism of modulating osteoclast differentiation could include induction of ROS. In the presence of the ROS-inducer PMA, nanobubble-dependent induction of ROS was potentiated, alongside an additional gas-dependent effect whereby NB-N_2 induced more ROS than either NB-O_2 or NB-air. Unfortunately, the gas-dependency could not be fully confirmed with RANKL, potentially due to more rapid and acute induction of ROS by RANKL than by the nanobubbles. As intracellular ROS are essential for osteoclast differentiation [34,35], it is possible that potentiation of RANKL-induced ROS by NB-N_2 could explain the greater overall osteoclast formation seen with these nanobubbles versus NB-O_2. In this regard, NB-N_2 may again mimic hypoxia with regards to osteoclast formation; ROS also being essential for effects of hypoxia on osteoclast differentiation [35].

The mechanisms described above might also contribute to effects of nanobubbles on osteoclast-mediated bone resorption. However, exposure of mature osteoclasts to nanobubbles for 24 h did not specifically affect bone resorption activity in this study. This was largely due to a high degree of variability in the data, although there was an indicative trend for NB-N_2 to increase bone resorption as also occurs in hypoxia [9–13]. It will be important in the future to investigate effects of nanobubbles on osteoclast biology in murine models of osteolytic disease.

It is interesting to speculate how orally-delivered oxygen-loaded nanobubbles might affect bone remodelling parameters *in vivo* and the mechanism(s) by which such effects could be mediated. Based on our *in vitro* data, it might be expected that oxygen-loaded nanobubbles would reduce the number of osteoclasts that form *in vivo* and, as a result, also reduce bone resorption despite having no direct effect on bone resorption itself. I*n vivo* studies would need to be conducted to address this balance, measuring bone resorption using high resolution X-ray computed tomography and circulating markers (e.g. CTX, P1NP) alongside assessment of osteoclast formation with immunohistochemistry for osteoclast-specific markers such as TRAP or CTSK. It is also

possible that the effect of NB-O_2 on osteoclasts within the complex microenvironment of the bone metastatic niche will differ from that *in vitro*.

Indeed, it is possible that the effect of NB-O_2 on bone-metastatic tumour tissue will differ from that observed by ourselves [25,26] and others [27,28] in primary tumours *in vivo*. Complex interactions between multiple cell types, as well as varied environmental stresses (e.g. hypoxia, pH, increased tissue pressure, etc), might impact both NB-cell interactions and the physiological effect(s) of these interactions. Specifically considering osteoclasts, it is worth noting that pH and hypoxia are not static states *in vivo* but modulate acutely due to variation in blood supply, metabolic activity and bone resorption activity among other factors. We acknowledge this as a limitation of the current work, which instead focussed on cell-type specific interactions of cells with NBs which might help deepen our understanding of the mechanism(s) of action of these agents.

The low calculated O_2-carrying capacity of the nanobubbles [26], together with the lack of effect on HIF and HIF-induced genes *in vitro*, leaves an alternative explanation required for observed effects on tumour reoxygenation and reduced HIF expression *in vivo* [25,27]. We have previously proposed that nanobubbles might increase the amount of oxygen available by passing into the bloodstream via the digestive tract, circulating and acting as extra carriers for oxygen absorbed during their passage through the lungs [26]. Lipid transfer of nanobubbles into endothelial cell membranes might also accelerate the rate of oxygen transport into the tumour matrix; either by directly shuttling oxygen dissolved inside them or by providing a higher diffusivity path. Such a mechanism(s) would explain why increased levels of oxygenation and reduced stabilisation of HIF protein are also observed with air- and argon-loaded nanobubbles *in vivo*, although not why the effect remains greater with NB-O_2 [25,26].

In comparison with healthy tissue, diseased bone is relatively hypoxic; healthy human mandibular bone has a pO_2 of 8.6% O_2 compared with 4% O_2 in osteoradionecrosis and 3.5% O_2 in chronic osteomyelitis [52] and the juxta-articular bone in rabbit models of osteoarthritis synovitis is also hypoxic [53]. Targeting the hypoxic microenvironment is therefore a prime treatment strategy in multiple skeletal conditions [54,55]. However, the bone microenvironment is complex and hypoxia also promotes the development and growth of the skeleton, including during fracture healing [56,57]. On balance, when osteoclast activation drives osteolytic disease, hypoxia enhances osteoclast-mediated bone resorption and inhibition of hypoxia pathways is considered a target. When osteoclasts are not overactive, hypoxia drives bone formation by promoting osteogenic-angiogenic coupling [13,58]. Given the propensity of NB-O_2 to inhibit osteoclast formation, via both increasing oxygen delivery and by lipid transfer-mediated suppression of cell-cell fusion, it will be a great interest in the future to investigate potential therapeutic effects of orally administered NB-O_2 on murine models of osteolytic disease.

6. Conclusions

In summary, we have systematically evaluated potential mechanism(s) whereby lecithin-based nanobubbles preferentially interact with cells of the mononuclear phagocyte system via lipid transfer, clathrin-dependent endocytosis and phagocytosis. This lecithin-dependent interaction led to general suppression of osteoclast differentiation via inhibition of cell fusion events during osteoclastogenesis. Additionally, fewer osteoclasts formed after repeat exposure to NB-O_2 than to NB-N_2. This effect was driven by differential early effects on the fusion of mononuclear precursor cells to form pre-osteoclasts, partly attributed to elevated potentiation of RANKL-induced ROS by NB-N_2. Overall, our findings suggest that oxygen-loaded nanobubbles could represent a promising therapeutic strategy for cancer therapy; reducing osteoclast formation and therefore bone metastasis via preferential interaction with monocytes/macrophages within the tumour and bone microenvironment in addition to known effects of directly improving tumour oxygenation.

CRediT authorship contribution statement

Helen J. Knowles: Conceptualization, Methodology, Validation, Formal analysis, Investigation, Data curation, Writing - original draft, Writing - review & editing, Visualisation. **Alexandra Vasilyeva:** Conceptualization, Investigation, Methodology. **Mihir Sheth:** Investigation, Formal analysis, Writing - review & editing. **Oliver Pattinson:** Methodology, Validation. **Jonathan May:** Investigation, Writing - review & editing. **Robin M.H. Rumney:** Conceptualization, Methodology, Supervision, Writing - review & editing. **Philippa A. Hulley:** Conceptualization, Methodology, Writing - review & editing. **Duncan B. Richards:** Conceptualization, Supervision, Funding acquisition. **Dario Carugo:** Supervision, Writing - review & editing. **Nicholas D. Evans:** Conceptualization, Writing - original draft, Writing - review & editing. **Eleanor Stride:** Conceptualization, Supervision, Project administration, Funding acquisition, Writing - review & editing.

Declaration of competing interest

The authors declare the following financial interests/personal relationships which may be considered as potential competing interests:

Data availability

Data will be made available on request.

Acknowledgements

This work was supported by funding from UK-SPINE (R52853/CN023), the EPSRC (EP/R013624/1, EP/R013594/1) and the National Institute for Health and Care Research (NIHR) Oxford Biomedical Research Centre (BRC). We also gratefully acknowledge the support of Gilberto Sayao da Silva whose donation to the University funded Mihir Sheth's salary. Many thanks to Dr Christoffer Lagerholm and Dr Emma Morris for technical assistance with confocal microscopy.

Appendix A. Supplementary data

Supplementary data to this article can be found online at https://doi.org/10.1016/j.biomaterials.2023.122448.

References

[1] Y. Zhuang, K. Liu, Q. He, X. Gu, C. Jiang, J. Wu, Hypoxia signaling in cancer: implications for therapeutic interventions, MedComm (2020) 4 (1) (2023) e203.
[2] B.P. Bui, P.L. Nguyen, K. Lee, J. Cho, Hypoxia-inducible factor-1: a novel therapeutic target for the management of cancer, drug resistance, and cancer-related pain, Cancers (Basel) 14 (24) (2022).
[3] T. Hiraga, Hypoxic microenvironment and metastatic bone disease, Int. J. Mol. Sci. 19 (11) (2018).
[4] H.J. Knowles, in: D. H (Ed.), Hypoxia-inducible factor (HIF)-mediated effects of the hypoxic niche in bone cancer, 3rd ed.Bone Cancer: Bone Sarcomas and Bone Metastases - from Bench to Bedside, Elsevier, 2022.
[5] R.E. Coleman, Clinical features of metastatic bone disease and risk of skeletal morbidity, Clin. Cancer Res. 12 (20 Pt 2) (2006), 6243s-9s.
[6] A. Maurizi, N. Rucci, The osteoclast in bone metastasis: player and target, Cancers (Basel) 10 (7) (2018).
[7] Y. Fujikawa, J.M. Quinn, A. Sabokbar, J.O. McGee, N.A. Athanasou, The human osteoclast precursor circulates in the monocyte fraction, Endocrinology 137 (9) (1996) 4058–4060.
[8] J.M. Quinn, J. Elliott, M.T. Gillespie, T.J. Martin, A combination of osteoclast differentiation factor and macrophage-colony stimulating factor is sufficient for both human and mouse osteoclast formation in vitro, Endocrinology 139 (10) (1998) 4424–4427.
[9] T.R. Arnett, D.C. Gibbons, J.C. Utting, I.R. Orriss, A. Hoebertz, M. Rosendaal, et al., Hypoxia is a major stimulator of osteoclast formation and bone resorption, J. Cell. Physiol. 196 (1) (2003) 2–8.
[10] M. Muzylak, J.S. Price, M.A. Horton, Hypoxia induces giant osteoclast formation and extensive bone resorption in the cat, Calcif. Tissue Int. 79 (5) (2006) 301–309.

[11] J.C. Utting, A.M. Flanagan, A. Brandao-Burch, I.R. Orriss, T.R. Arnett, Hypoxia stimulates osteoclast formation from human peripheral blood, Cell Biochem. Funct. 28 (5) (2010) 374–380.
[12] H.J. Knowles, N.A. Athanasou, Acute hypoxia and osteoclast activity: a balance between enhanced resorption and increased apoptosis, J. Pathol. 218 (2) (2009) 256–264.
[13] H.J. Knowles, Hypoxic regulation of osteoclast differentiation and bone resorption activity, Hypoxia 3 (2015) 73–82.
[14] T. Hiraga, S. Kizaka-Kondoh, K. Hirota, M. Hiraoka, T. Yoneda, Hypoxia and hypoxia-inducible factor-1 expression enhance osteolytic bone metastases of breast cancer, Cancer Res. 67 (9) (2007) 4157–4163.
[15] P.A. Hulley, T. Bishop, A. Vernet, J.E. Schneider, J.R. Edwards, N.A. Athanasou, et al., Hypoxia-inducible factor 1-alpha does not regulate osteoclastogenesis but enhances bone resorption activity via prolyl-4-hydroxylase 2, J. Pathol. 242 (3) (2017) 322–333.
[16] P.A. Hulley, I. Papadimitriou-Olivgeri, H.J. Knowles, Osteoblast-osteoclast coculture amplifies inhibitory effects of FG-4592 on human osteoclastogenesis and reduces bone resorption, JBMR Plus 4 (7) (2020) e10370.
[17] T. Takemori, T. Kawamoto, T. Ueha, M. Toda, M. Morishita, E. Kamata, et al., Transcutaneous carbon dioxide application suppresses bone destruction caused by breast cancer metastasis, Oncol. Rep. 40 (4) (2018) 2079–2087.
[18] C. Reynaud, L. Ferreras, P. Di Mauro, C. Kan, M. Croset, E. Bonnelye, et al., Lysyl oxidase is a strong determinant of tumor cell colonization in bone, Cancer Res. 77 (2) (2017) 268–278.
[19] L. Fournier, T. de La Taille, C. Chauvierre, Microbubbles for human diagnosis and therapy, Biomaterials 294 (2023) 122025.
[20] J.N. Kheir, L.A. Scharp, M.A. Borden, E.J. Swanson, A. Loxley, J.H. Reese, et al., Oxygen gas-filled microparticles provide intravenous oxygen delivery, Sci. Transl. Med. 4 (140) (2012) 140ra88.
[21] J.A. Feshitan, N.D. Legband, M.A. Borden, B.S. Terry, Systemic oxygen delivery by peritoneal perfusion of oxygen microbubbles, Biomaterials 35 (9) (2014) 2600–2606.
[22] J.R. Eisenbrey, L. Albala, M.R. Kramer, N. Daroshefski, D. Brown, J.B. Liu, et al., Development of an ultrasound sensitive oxygen carrier for oxygen delivery to hypoxic tissue, Int. J. Pharm. 478 (1) (2015) 361–367.
[23] R. Song, D. Hu, H.Y. Chung, Z. Sheng, S. Yao, Lipid-polymer Bilaminar oxygen nanobubbles for enhanced Photodynamic therapy of cancer, ACS Appl. Mater. Interfaces 10 (43) (2018) 36805–36813.
[24] N. Gombodorj, T. Yokobori, N. Mutsuki, B. Erkhem-Ochir, H. Okami, T. Asao, et al., Effects of ultrafine single-nanometer oxygen bubbles on radiation sensitivity in a tumor-bearing mouse model, Int. J. Mol. Sci. 23 (12) (2022).
[25] J. Owen, C. McEwan, H. Nesbitt, P. Bovornchutichai, R. Averre, M. Borden, et al., Reducing tumour hypoxia via oral administration of oxygen nanobubbles, PLoS One 11 (12) (2016) e0168088.
[26] J. Owen, K. Logan, H. Nesbitt, S. Able, A. Vasilyeva, E. Bluemke, et al., Orally administered oxygen nanobubbles enhance tumor response to sonodynamic therapy, Nano Select (2021) 1–8.
[27] A. Mahjour, M. Khazaei, E. Nourmohammadi, H. Khoshdel-Sarkarizi, A. Ebrahimzadeh-Bideskan, H.R. Rahimi, et al., Evaluation of antitumor effect of oxygen nanobubble water on breast cancer-bearing BALB/c mice, J. Cell. Biochem. 120 (9) (2019) 15546–15552.
[28] P.N. Bhandari, Y. Cui, B.D. Elzey, C.J. Goergen, C.M. Long, J. Irudayaraj, Oxygen nanobubbles revert hypoxia by methylation programming, Sci. Rep. 7 (1) (2017) 9268.
[29] D.G. King, E. Stride, J. Mendis, W.H. Gurton, H. Macrae, L. Jones, et al., A double-blind, randomized, placebo-controlled pilot study examining an oxygen nanobubble beverage for 16.1-km time trial and repeated sprint cycling performance, J. Diet. Suppl. (2023) 1–15.
[30] C. Kelly, C. Jefferies, S.A. Cryan, Targeted liposomal drug delivery to monocytes and macrophages, J. Drug Deliv. 2011 (2011) 727241.
[31] L. Ottaviano, K.L. Schaefer, M. Gajewski, W. Huckenbeck, S. Baldus, U. Rogel, et al., Molecular characterization of commonly used cell lines for bone tumor research: a trans-European EuroBoNet effort, Gene Chromosome Cancer 49 (1) (2010) 40–51.
[32] J. Takito, M. Nakamura, Heterogeneity and actin cytoskeleton in osteoclast and macrophage multinucleation, Int. J. Mol. Sci. 21 (18) (2020).
[33] L. Schito, G.L. Semenza, Hypoxia-inducible factors: master regulators of cancer progression, Trends Cancer 2 (12) (2016) 758–770.
[34] H.S. Kim, S.T. Nam, S.H. Mun, S.K. Lee, H.W. Kim, Y.H. Park, et al., DJ-1 controls bone homeostasis through the regulation of osteoclast differentiation, Nat. Commun. 8 (1) (2017) 1519.
[35] T.S. Agidigbi, C. Kim, Reactive oxygen species in osteoclast differentiation and possible pharmaceutical targets of ROS-mediated osteoclast diseases, Int. J. Mol. Sci. 20 (14) (2019).
[36] Y. Wang, X. Liu, W. Huang, J. Liang, Y. Chen, The intricate interplay between HIFs, ROS, and the ubiquitin system in the tumor hypoxic microenvironment, Pharmacol. Ther. 240 (2022) 108303.
[37] G. Sahay, D.Y. Alakhova, A.V. Kabanov, Endocytosis of nanomedicines, J. Contr. Release 145 (3) (2010) 182–195.
[38] S.E. Gratton, P.A. Ropp, P.D. Pohlhaus, J.C. Luft, V.J. Madden, M.E. Napier, et al., The effect of particle design on cellular internalization pathways, Proc. Natl. Acad. Sci. U. S. A. 105 (33) (2008) 11613–11618.
[39] D. Carugo, M. Aron, E. Sezgin, J. Bernardino de la Serna, M.K. Kuimova, C. Eggeling, et al., Modulation of the molecular arrangement in artificial and biological membranes by phospholipid-shelled microbubbles, Biomaterials 113 (2017) 105–117.
[40] G.R. Gulino, C. Magnetto, A. Khadjavi, A. Panariti, I. Rivolta, M. Soster, et al., Oxygen-loaded nanodroplets effectively abrogate hypoxia dysregulating effects on secretion of MMP-9 and TIMP-1 by human monocytes, Mediat. Inflamm. 2015 (2015) 964838.
[41] S. Jeganathan, C. Fiorino, U. Naik, H.S. Sun, R.E. Harrison, Modulation of osteoclastogenesis with macrophage M1- and M2-inducing stimuli, PLoS One 9 (8) (2014) e104498.
[42] C. Dou, N. Ding, C. Zhao, T. Hou, F. Kang, Z. Cao, et al., Estrogen deficiency-mediated M2 macrophage osteoclastogenesis contributes to M1/M2 ratio alteration in ovariectomized osteoporotic mice, J. Bone Miner. Res. 33 (5) (2018) 899–908.
[43] S.D. Neale, D.R. Haynes, D.W. Howie, D.W. Murray, N.A. Athanasou, The effect of particle phagocytosis and metallic wear particles on osteoclast formation and bone resorption in vitro, J. Arthroplasty 15 (5) (2000) 654–662.
[44] S.K. Verma, E. Leikina, K. Melikov, C. Gebert, V. Kram, M.F. Young, et al., Cell-surface phosphatidylserine regulates osteoclast precursor fusion, J. Biol. Chem. 293 (1) (2018) 254–270.
[45] J.H. Kang, H.M. Ko, G.D. Han, S.Y. Lee, J.S. Moon, M.S. Kim, et al., Dual role of phosphatidylserine and its receptors in osteoclastogenesis, Cell Death Dis. 11 (7) (2020) 497.
[46] R.P. Richter, J.L. Him, B. Tessier, C. Tessier, A.R. Brisson, On the kinetics of adsorption and two-dimensional self-assembly of annexin A5 on supported lipid bilayers, Biophys. J. 89 (5) (2005) 3372–3385.
[47] M. Torres, S. Parets, J. Fernandez-Diaz, R. Beteta-Gobel, R. Rodriguez-Lorca, R. Roman, et al., Lipids in pathophysiology and development of the membrane lipid therapy: new bioactive lipids, Membranes (Basel) 11 (12) (2021).
[48] T. Huang, Y. Wang, Z. Yu, X. Miao, Z. Jiang, K. Yu, et al., Effect of mitophagy in the formation of osteomorphs derived from osteoclasts, iScience 26 (5) (2023) 106682.
[49] M.M. McDonald, W.H. Khoo, P.Y. Ng, Y. Xiao, J. Zamerli, P. Thatcher, et al., Osteoclasts recycle via osteomorphs during RANKL-stimulated bone resorption, Cell 184 (7) (2021) 1940.
[50] M.S. Khan, J. Hwang, K. Lee, Y. Choi, Y. Seo, H. Jeon, et al., Anti-Tumor drug-loaded oxygen nanobubbles for the degradation of HIF-1alpha and the upregulation of reactive oxygen species in tumor cells, Cancers (Basel) 11 (10) (2019).
[51] M.S. Khan, J. Hwang, Y. Seo, K. Shin, K. Lee, C. Park, et al., Engineering oxygen nanobubbles for the effective reversal of hypoxia, Artif. Cells, Nanomed. Biotechnol. 46 (sup3) (2018) S318–S327.
[52] P. Maurer, L. Meyer, A.W. Eckert, M. Berginski, J. Schubert, Measurement of oxygen partial pressure in the mandibular bone using a polarographic fine needle probe, Int. J. Oral Maxillofac. Surg. 35 (3) (2006) 231–236.
[53] H. Kofoed, Synovitis causes hypoxia and acidity in synovial fluid and subchondral bone, Injury 17 (6) (1986) 391–394.
[54] E.M. Sabi, A. Singh, Z.M. Althafar, T. Behl, A. Sehgal, S. Singh, et al., Elucidating the role of hypoxia-inducible factor in rheumatoid arthritis, Inflammopharmacology 30 (3) (2022) 737–748.
[55] M. Pierrevelcin, Q. Fuchs, B. Lhermitte, M. Messe, E. Guerin, N. Weingertner, et al., Focus on hypoxia-related pathways in pediatric osteosarcomas and their druggability, Cells 9 (9) (2020).
[56] C.T. Brighton, A.G. Krebs, Oxygen tension of healing fractures in the rabbit, J. Bone Joint Surg. 54 (2) (1972) 323–332.
[57] D.K. Taheem, G. Jell, E. Gentleman, Hypoxia inducible factor-1alpha in osteochondral tissue engineering, Tissue Eng., Part B 26 (2) (2020) 105–115.
[58] X. Huang, Y. Zhang, B. Qi, K. Sun, N. Liu, B. Tang, et al., HIF-1alpha: Its notable role in the maintenance of oxygen, bone and iron homeostasis (Review), Int. J. Mol. Med. 50 (6) (2022).